Wearable, Ultrawide-Range, and Bending-Insensitive Pressure Sensor Based on Carbon Nanotube Network-Coated Porous Elastomer Sponges for Human Interface and Healthcare Devices

Wearable, Ultrawide-Range, and Bending-Insensitive Pressure Sensor based on Carbon Nanotube Network-Coated Porous Elastomer Sponges for Human Interface and Healthcare Devices

Seunghwan Kim, [a] *Morteza Amjadi,* [b] *Tae-Ik Lee,* [a] *Yongrok Jeong,* [a] *Donguk Kwon,* [a] *Min Seong Kim,* [a] *Kyuyoung Kim, Taek-Soo Kim,* [a] *Yong Suk Oh*,*[a, c] *and Inkyu Park*,* [a]

[a] Department of Mechanical Engineering, Korea Advanced Institute of Science and Technology (KAIST), 291 Daehak-ro, Yuseong-gu, Daejeon, 305-701, South Korea

[b] Physical Intelligence Department Max-Planck Institute for Intelligent Systems Heisenbergstr. 3 Stuttgart 70569, Germany

[c] Center for Bio-Integrated Electronics (CBIE), Northwestern University, Evanston, Illinois 60208, United States

KEYWORDS

carbon nanotube, microporous elastomer, flexible pressure sensor, ultrawide pressure range, bending-insensitivity, human interface device

ABSTRACT

Flexible and wearable pressure sensors have attracted tremendous attention due to their wider applications such as human-interfacing and healthcare monitoring. However, it is a great challenge to achieve accurate pressure detection and stability against external stimuli (in particular, bending deformation) over a wide range of pressure from tactile to body weight levels. Here, we introduce an ultrawide-range, bending-insensitive, and flexible pressure sensor based on a carbon nanotube (CNT) network-coated thin porous elastomer sponge for use in human interface devices. The integration of the CNT networks into three dimensional (3D) microporous elastomers provides high deformability and a large change of contact between the conductive CNT networks due to the presence of micropores, thereby improving the sensitivity compared with that obtained using CNTs-embedded solid elastomers. As electrical pathways are continuously generated up to high compressive strain (~80%), the pressure sensor shows an ultrawide pressure-sensing range (10 Pa–1.2 MPa) while maintaining favorable sensitivity (0.01–0.02 kPa^{-1}) and linearity (R^2 ~0.98). Also, the pressure sensor exhibits excellent electromechanical stability and insensitivity to bending-induced deformations. Finally, we demonstrate that the pressure sensor can be applied in a flexible piano pad as an entertainment human interface device and a flexible foot insole as a wearable healthcare and gait monitoring device, respectively.

INTRODUCTION

Flexible and wearable pressure sensors have received tremendous attentions due to their great potential for a variety of applications, including artificial electronic skins,[1–4] soft robotics,[5–7] healthcare monitoring/diagnosis,[8–10] energy harvesting,[11–13] and human interface devices.[14,15] Next-generation flexible pressure sensors are required to precisely detect a wide

range of pressure (low-pressure regime of 0–10 kPa, medium-pressure regime of 10–100 kPa, and high-pressure regime of >100 kPa) with high sensitivity and reliability for use in human body monitoring systems.[10,16]

In general, the flexible pressure sensors are mainly divided into resistive, capacitive and piezoelectric types according to the pressure sensing mechanisms. Among them, the resistive pressure sensors have been intensively investigated owing to several advantages such as simple device structures, easy signal read-out, and high pixel resolution.[10,17] Conventionally, flexible pressure sensors have been fabricated using a method for embedding conductive nanomaterials (*e.g.* carbon blacks, carbon nanotubes, *etc*.) into polymer or elastomer matrix (*e.g.* PDMS, Ecoflex, polyurethane, *etc.*). These types of pressure sensors, however, suffered from low sensitivity and poor hysteresis over wide ranges of pressure due to an imperfect recovery of the conductive nanomaterial networks and inherent viscoelasticity of the matrix materials, thereby limiting their practical applications.[7,18,19] Several strategies have been proposed to improve the performance of the flexible pressure sensors using a variety of two dimensional (2D) micro/nano-structured active layers, including conductive polymer-coated micropyramid arrays,[20] electrospun nanofiber-based thin films,[21] and assembly of two interlocked metal-deposited nanofiber arrays.[22] The flexible pressure sensors based on the 2D micro/nano-structured active layers showed excellent sensitivity and quick response in a low pressure range (generally, < 10kPa) owing to fine contacts between the conductive micro/nano-structures. However, they suffered from expensive, time-consuming, and complicated process steps (*e.g.* photolithography, etching, and electrospinning). Furthermore, they exhibit only small ranges of measurable pressure due to the limited deformation of the 2D micro/nano-structures.

Alternatively, microscale porous sponge-like materials combined with 3D conductive networks have been suggested as the active layers of the flexible pressure sensors due to both electrical conductivity and mechanical durability. The 3D conductive sponge-like active layers

were typically fabricated using a coating process or a direct synthesis of the conductive nanomaterials (*e.g.* metal nanowires, graphenes, and CNTs, *etc.*) on porous backbones. For example, highly sensitive pressure sensors based on gold nanowires-coated fabric papers,[23] graphene-coated microfractured polyurethane films,[24] reduced graphene oxide (synthesized by chemical vapor deposition)-coated PDMS foams,[25] and CNT/silver nanoparticles-coated commercial sponges[26] have been reported. Among them, CNT-coated porous PDMS sponges are one of the most promising candidates for use in human interfacing applications because of intrinsic flexibility, skin-like modulus of the PDMS sponge, and high electrical conductivity of the CNTs. A highly porous and compressible CNT-PDMS sponge fabricated using a simple and cost-effective sugar template-assisted technique was first developed by Han *et al*.[27] Also, a pressure sensor based on a CNT-PDMS sponge, reported by Iglio *et al*., showed the capability of pressure sensing in the pressure range up to medium regime.[28] However, an integration of the CNT-PDMS sponge-based pressure sensors into human interface devices has not been demonstrated yet. There are two important challenges for use in practical human interfacing applications. Firstly, various sensing parameters (*e.g*. sensitivity, hysteresis, dynamic response, *etc.*) of the pressure sensors should be evaluated over a wide range of dynamic pressure. Secondly, the stability of the pressure sensors should be maintained even under unintended stimuli (in particular, bending deformation).[29]

Herein, we introduce an ultrawide-range, bending-insensitive, and flexible resistive pressure sensor based on a CNT network-coated thin porous PDMS sponge (CCPPS) integrated with two bottom electrodes for use in human interface devices. In order to investigate its suitability in practical applications, pressure-sensing performances of the CCPPS-based pressure sensor were evaluated under static and dynamic conditions. The CCPPS-based pressure sensor exhibited an ultrawide pressure sensing range from 10 Pa to 1.2 MPa while maintaining favorable sensitivity, due to continuous generation of electrical pathways with contact between

the serially stacked CNT-coated micropores even over wide compression levels. Reversible, instant, and robust closure/opening behavior of the micropores within the CCPPS led to low hysteresis, good dynamic response, and long-term reliability of the pressure sensor. Also, the CCPPS-based pressure sensor exhibited a bending-insensitive pressure-sensing capability, which can lead to an accurate detection of the normal pressure even on curved or dynamic surfaces. To the best of our knowledge, this is the first to study the properties of nanomaterials-coated porous sponges-based pressure sensors under various bent conditions. Finally, the utility of the CCPPS-based flexible pressure sensor was demonstrated for a flexible piano pad and a flexible foot insole, respectively.

EXPERIMENTAL SECTION

Preparation of a CNT network-coated porous PDMS sponge (CCPPS). A sugar template (15 mm × 15 mm × 15 mm) was immersed in degassed PDMS prepolymer (Sylgard 184, Dow Corning Co., USA, mass ratio of matrix and curing agent = 10 : 1). The liquid PDMS prepolymer was infiltrated into the sugar template in a vacuum chamber for 1 h, and then was cured in a convection oven at 70 °C for 2 h. The composite of sugar and cured PDMS was cut into a thin slice with a thickness of ~3 mm using a sandpaper, and immersed in deionized water at 60 °C for 1 h to dissolve the sugar portion for the fabrication of a porous PDMS sponge (PPS, 15 mm × 15 mm × 3 mm). Then, the obtained PPS was treated with an oxygen plasma for 10 minutes. 0.25 g of multi-walled carbon nanotubes (MWCNTs, Hyosung, Korea, diameter = 16 ± 3.6 nm, length = 5–20 μm) was dispersed in 100 ml of isopropyl alcohol (IPA). After vortex mixing for 1 h, an ultra-sonication was carried out for 1 h to prepare homogeneous 0.25wt% CNT-IPA dispersion. The plasma-treated PPS was immersed in the CNT-IPA dispersion and repeatedly squeezed for CNT coating on the surfaces of the PDMS backbone. After complete evaporation of the IPA solvent, the prepared CCPPS was rinsed in DI water

and dried in a convection oven at 50 °C for 1 h. For comparison, a 0.3 wt% CNT-embedded solid PDMS (15 mm × 15 mm × 3mm), which has similar resistance level with that of the CCPPS, was also fabricated. The MWCNTs was mixed with the PDMS prepolymer (mass ratio of MWCNT and PDMS = 0.3 : 99.7) using a planetary centrifugal mixer (ARE-310, Thinky, Japan) to prepare a homogeneous mixture. After curing of the PDMS prepolymer in a convection oven at 70 °C for 2 h, a CNT-embedded PDMS was fabricated.

Preparation of a CCPPS-based pressure sensor. Two flexible copper sheets (thickness = ~50 μm) were attached on a flexible PET film (thickness = ~50 μm) for the fabrication of two bottom electrodes. The CCPPS was bonded to the electrodes using a silver paste adhesive to prepare a CCPPS-based pressure sensor. Then, the silver paste was annealed in a convection oven at 120 °C for 30 min.

Characterization of a CCPPS-based pressure sensor. The surface and cross-sectional morphology of the CCPPS were characterized by a field emission scanning electron microscopy (FE-SEM, Sirion, FEI, Hillsboro, USA) and an optical microscopy (VH-Z100R, Keyence, Japan). The internal cross-sectional geometries of the CCPPS were investigated using a nondestructive microcomputed tomography (Micro CT, SKYSCAN 1272, Bruker, USA). A tensile/compression testing machine (C224-E053D Autograph AG-X Plus, Shimadzu, Japan) capable of precise control of load and displacement was used to characterize pressure responses of the CCPPS-based pressure sensor. Force and electrical current data were collected using a load cell (Load Cell SLBL, Shimadzu, Japan) and a source meter (Keithley 2400, Keithley instruments, USA), respectively.

Preparation of a flexible piano pad. At first, piano keyboard-shaped molds, which have empty spaces (15 mm × 15 mm × 3 mm), were manufactured using a 3D printer. Ecoflex prepolymer (Ecoflex 0030, Smooth-On, USA, mass ratio of matrix A and B = 1 : 1) was poured into the molds, and cured in a convection oven at 80 °C for 2 h, for the formation of the

keyboard housings. Voltage dividing circuit consisting of the CCPPS-based pressure sensor and a reference resistance was integrated into an empty space of each keyboard housing for the preparation of 13 keyboard components (8 white keys and 5 black keys, from Do; C4 to Do; C5). Each keyboard component was bonded in an array configuration using a silicone adhesive to form a flexible piano pad. The electrical circuits were connected to a data acquisition (DAQ) board and PC where sound midi files were programmed.

Preparation of a flexible foot insole. Ten CCPPS-based pressure sensors were attached on a flexible printed circuit board (FPCB, thickness = ~100 μm), and the electrode pairs were connected to the exposed electrical circuit of the FPCB. The sensor-integrated FPCB was combined with a cover insole layer with socket structures for completion of a flexible foot insole. The electrical circuits were connected to a DAQ board and PC where a real-time 3D mapping was programmed for real-time measurement.

RESULTS AND DISCUSSION

Figure 1a shows a schematic illustration of overall fabrication procedures of a flexible resistive pressure sensor, which is composed of a CNT network-coated thin porous PDMS sponge (CCPPS) and two bottom electrodes. The CCPPS was fabricated by the following steps (Detailed information is described in Experimental Section): (1) fabrication of a porous PDMS sponge (PSS) using a sugar template; (2) oxygen plasma treatment to the PPS; (3) CNT coating of the plasma-treated PPS using a dip-coating method for the preparation of a CCPPS (Figure S1a). Figure S1b and Figure S1c show photographic images of the PPS and the CCPPS, respectively. The white color of the PPS was changed to the black color due to the deposition of the CNTs. In Figure S1d, a slice of the CCPPS cut in half shows that the CNTs were evenly coated inside the PPS. Figure 1b shows a photographic image of the CCPPS-based pressure sensor. It should be noted that the two bottom electrodes are designed for efficient and stable

integration of the three dimensional (3D) sensors to 2D electrical circuits for practical human interfacing applications. Moreover, the pressure sensor with a thickness lower than 3 mm provides an excellent flexibility, which is one of the import factors for human monitoring and wearable applications, as shown in Figure 1c. The pressure sensor was not damaged under various bent conditions. In Figure 1d and 1e, a SEM image and a magnified SEM image show that the surface morphology of the CCPPS is porous configuration. The size of the micropores is distributed in the range of 300–500 μm, and the porosity was calculated as 73 ± 0.6% (Detailed information is described in Table S1). By comparing the SEM images of the surface morphology of the CCPPS and a bare porous PDMS backbone (Figure S1e), it was concluded that complex CNT layers were coated on the 3D-interconnected micropores and resulted in the formation of conductive networks. In the micro CT image (Movie S1), it was observed that the micropores were consistently distributed over the entire volume of the CCPPS.

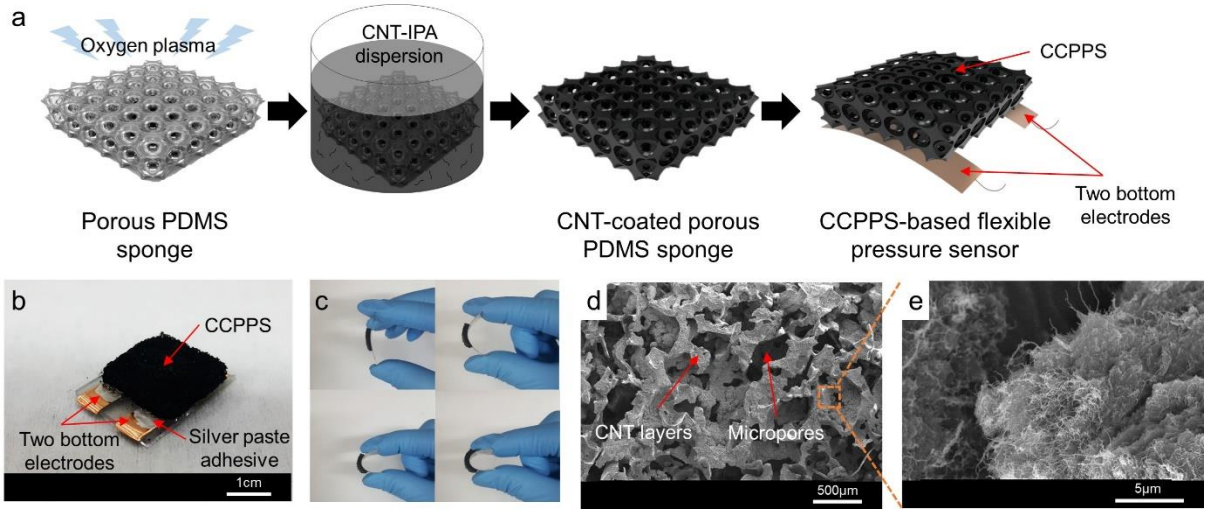

Figure 1 Fabrication and morphology of a CCPPS-based flexible pressure sensor: (a) Schematic illustration of overall fabrication procedures of the pressure sensor; (b) A photographic image of the pressure sensor composed of a CCPPS as an active layer and two bottom electrodes; (c) Photographic images of the pressure sensor under bent conditions,

showing excellent flexibility and structural durability; (d) SEM image of surface morphology of the CCPPS and (e) Magnified SEM image of CNT layers coated on the porous PDMS backbone, forming conductive networks.

Figure 2a shows a schematic illustration of pressure sensing mechanism of the CCPPS-based flexible pressure sensor. An initial current (I_o) flows through electrical percolation paths along the 3D-interconnected CNT networks (red arrow). Under compressive loading, the current increases from I_o to I_f due to additional electrical paths (yellow arrow) according to an increase of contact area between the CNT networks during gradual closure of the micropores. In Figure 2b, cross-sectional SEM images of the CCPPS at compression of 0, 40, and 80 % clearly show the formation of overlapped CNT layers upon the compression of the CCPPS (the same regions are marked with red circles). Movie S2 shows a gradual geometrical change of the microporous configuration of the CCPPS during several compression/release cycles (0–80–0%) in a more detail. It should be noted that even at the compression larger than 60%, the new electrical paths between the CNT networks were continuously generated owing to the presence of relatively small-sized remaining micropores, which can lead to an enough current change even in a high pressure range. Figure S2a shows reversible closure/opening behavior of the micropores with elastic deformation of PDMS bridges surrounding the micropores. Also, almost perfect recovery of the initial states without noticeable structural changes after the several compression/release cycles was shown in Figure S2b. In Figure S3, the CCPPS exhibited a negligible barreling phenomenon, which is a lateral volume expansion, up to a compression of 80%. The anti-barreling property of the CCPPS leads to preventing an electrical and physical interference between adjacent sensors for high resolution array configurations.

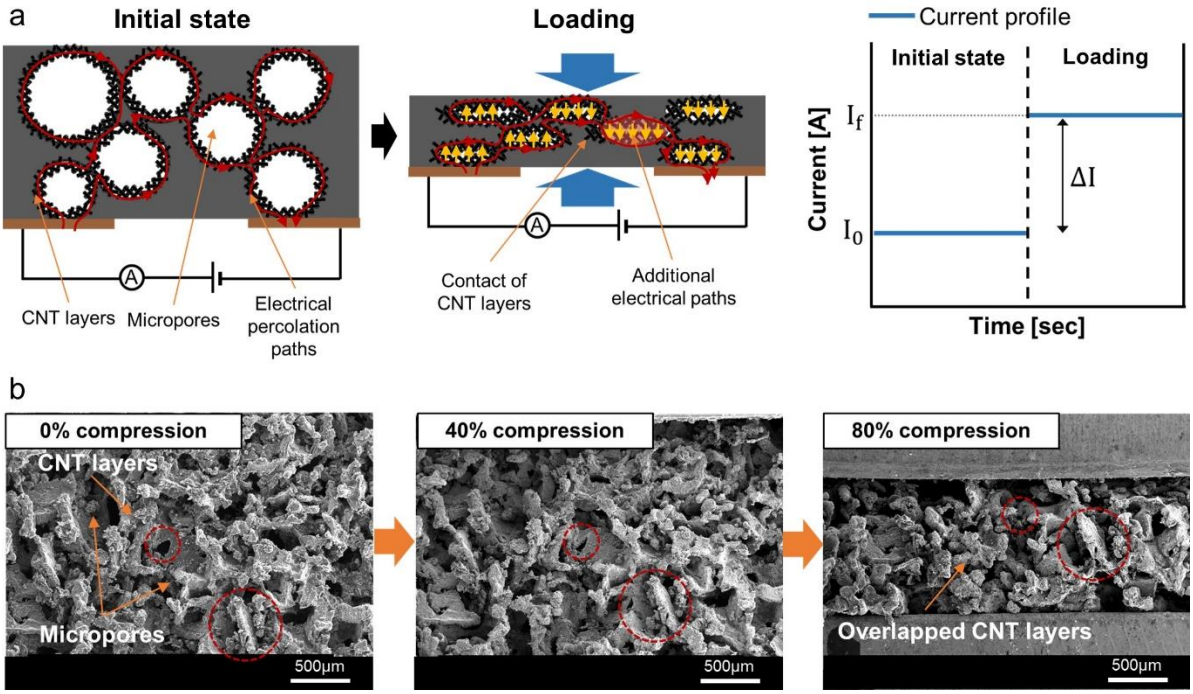

Figure 2 (a) Schematic illustration of pressure sensing mechanism of the CCPPS-based flexible pressure sensor: Increase of a current from I_o to I_f is induced by additional contact between CNT networks under compressive loading; (b) Cross-sectional SEM images of the CCPPS at compression of 0, 40, and 80%, showing the formation of overlapped CNT layers upon the compression of the CCPPS.

The performance factors of the CCPPS-based flexible pressure sensor that are important for practical applications to human interface devices were systematically evaluated under various static and dynamic loading conditions. Figure 3a compares normalized current changes ($\Delta I/I_o$) as a function of applied pressures of the pressure sensors based on the CCPPS and a CNT-embedded solid PDMS in a pressure range up to ~1.2 MPa. The sensitivity is defined as $S = \delta (\Delta I / I_o) / \delta P$, where P denotes the applied pressure, and I_o and ΔI mean the initial current and the current change, respectively. It is noted that the P *vs.* $\Delta I/I_o$ curve of the CCPPS-based pressure sensor is classified into two regions according to the sensitivity. In the first region (0

≤ P ≤ 100 kPa, 0 ≤ compressive strain (ε_c) ≤ 60%, black curve), the CCPPS-based pressure sensor exhibited a sensitivity (S_1) of ~0.02 kPa^{-1}, which is much higher than that of the pressure sensor based on the CNT-embedded solid PDMS (S_c of ~0.0004 kPa^{-1}, green curve). The sensitivity improvement in the low pressure range is based on the following characteristics of the microporous configuration of the CCPPS: (i) A large increase of the contact between the 3D-interconnected CNT networks deposited on the micropores, and (ii) low mechanical stiffness due to the presence of the micropores (~30 times lower than that of the CNT-embedded solid PDMS, Figure S4a) which induce more compressive deformability. These factors can generate large current changes even under small external forces. In the second region (100 kPa ≤ P ≤ 1.2 MPa, 60% ≤ ε_c ≤ 80%, red curve), the CCPPS-based pressure sensor exhibited a sensitivity (S_2) of ~0.01 kPa^{-1}, which is lower than S_1 due to gradual closure of the micropores. However, it is noticed that a dramatic saturation of the sensitivity was not observed, since new contact between the CNT networks were continuously created over the wide pressure range (as already observed in Movie S2). The value of S_2 is still higher than those of previously reported pressure sensors working in the high pressure range (0.0009 kPa^{-1} and 0.0023 kPa^{-1}, *etc.*) [25,30,31]. High linearity (R^2 ~0.98) was also shown in the entire pressure range. Figure S4b shows the detection capability of ultralow pressure levels (10 and 50Pa). Accordingly, the CCPPS-based pressure sensor exhibits an ultrawide sensing range from ultralow to high pressures (10 Pa–1.2 MPa) which covers the whole human tactile and body weight levels, with favorable sensitivity (0.01–0.02 kPa^{-1}) maintained. As shown in Figure S4c, there was no noticeable difference between pressure responses at different compression rates from 0.2 to 1.0 mm/sec. This result indicates that the pressure responses of the CCPPS-based pressure sensor would not vary under diverse dynamic stimuli. Figure 3b shows the hysteresis characteristics of the CCPPS-based pressure sensor for various compression levels of 20, 40, 60, and 80%. The pressure sensor exhibited low hysteresis (7.3 % for 0–100 kPa and 5.7 % for

0–1000 kPa) with a complete recovery of the initial states over the ultrawide pressure range up to ~1MPa, which originates from the reversible closure/opening behavior of the micropores of the CCPPS (As already observed in Figure S2). Moreover, as shown in Figure 3c, dynamic sensing properties of the CCPPS-based pressure sensor were evaluated under several loading-holding-unloading dynamic cycles at different pressure levels of 0–10 kPa, 10–100 kPa, and 100–1000 kPa, respectively. The pressure sensor can be used to detect different pressure levels with high resolution over the wide ranges of pressures up to ~1MPa. As shown in Figure 3d and S4d, $\Delta I/I_o$ (blue curve) could instantly respond to input loads (black curve; measured by a load cell) with no remarkable time delays during the step loading and step unloading, respectively. The response times (~8.5 ms for loading and ~10 ms for unloading) were defined as a difference between 90% rising times ($\Delta\tau_{90\%}$) of the two curves. The fast response of the pressure sensor facilitates a real-time pressure measurement under dynamic stimuli. Furthermore, long-term reliability of pressure sensors is one of the important parameters for use in practical applications. As shown in Figure 3e, the CCPPS-based pressure sensor exhibited excellent electromechanical reliability without noticeable instability or failures during 1000 repetitive compression/release cycles. In the magnified curves (inset), it is observed that stable and repeatable responses were maintained after 100 cycles. These results can offer the possibility of the CCPPS-based flexible pressure sensor to monitor dynamic human motions over an ultrawide pressure range.

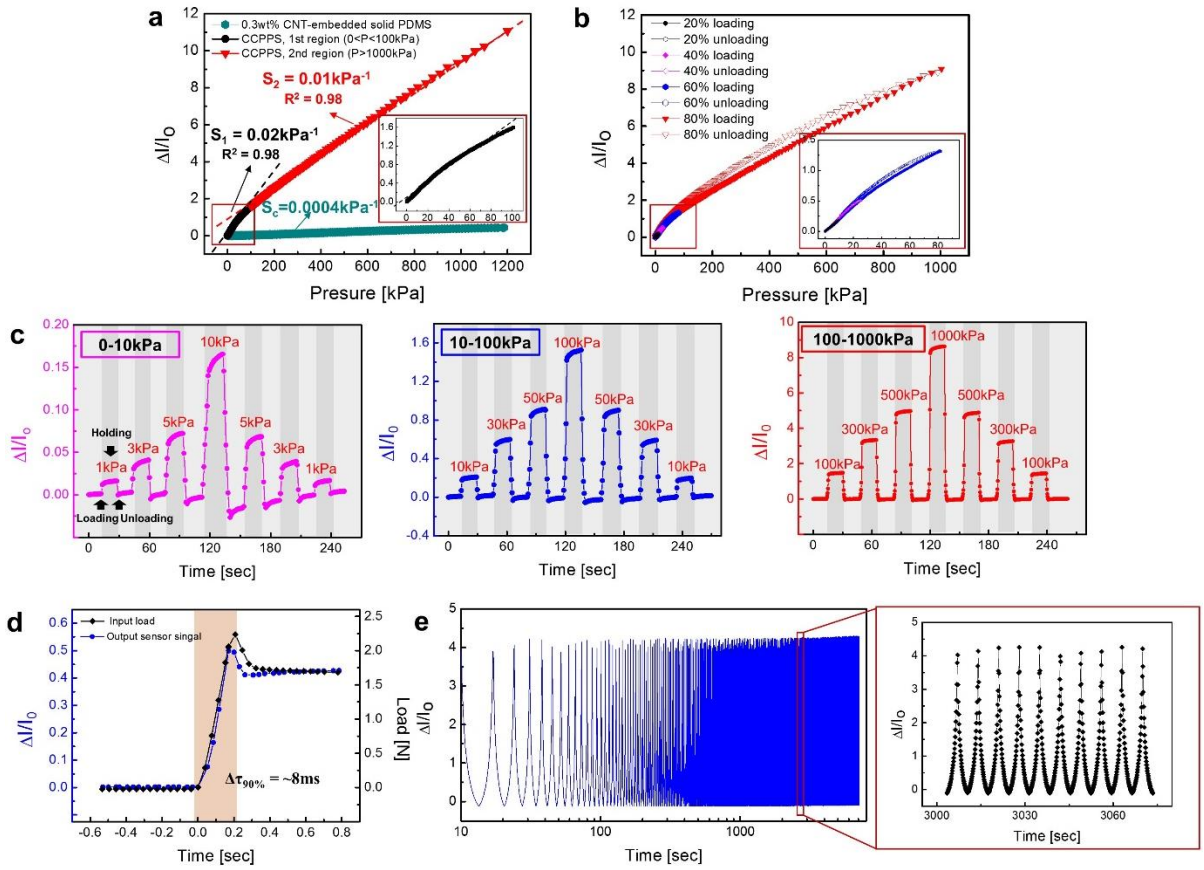

Figure 3 Performance of a CCPPS-based flexible pressure sensor: (a) Pressure response curves of the pressure sensor based on the CCPPS and a CNT-embedded solid PDMS; (b) Hysteresis characteristics of the pressure sensor at various compression levels; (c) Dynamic responses of the pressure sensor at different pressure levels: 0–10 kPa, 10–100 kPa, and 100–1000 kPa; (d) Transient response of the pressure sensor under a step loading. (e) Long-term reliability of the pressure sensor during 1,000 repetitive compression/release (ε_c = 0–75%) cycles.

As bending deformation can be applied to pressure sensors attached on human bodies, the flexible and wearable pressure sensors are required to provide the electromechanical stability under both flat and curved surfaces. Bending effects on the performance of the CCPPS-based flexible pressure sensor were investigated as shown in Figure 4. In order to evaluate the characteristics of bending-insensitivity, the CCPPS-based pressure sensor was attached to the

curved surfaces of supports with different bending radii ($r_{bending}$) ranged from 50 mm to 7.5 mm as shown in Figure S5a. As shown in Figure 4a, for both cases of electrodes ∥ bending (*i.e.* the electrode pairs are aligned in parallel to the longitudinal plane where opposite couple moments are acting) and electrodes ⊥ bending (*i.e.* the electrode pairs are aligned in perpendicular to the longitudinal plane), the base resistance (R_{base}) remained almost constant at different values of $r_{bending}$ as shown in Figure 4a. The maximum normalized base resistance change ($\Delta R_{base}/R_{base,o}$) was measured to be within ~5%. In Figure S5b, cross-sectional SEM images compare the microporous morphologies of the CCPPS with various $r_{bending}$. Despite the entire sensor structure being bent up to $r_{bending}$ of 7.5 mm, there was no significant current change due to negligible changes of contact between the CNT networks. The bending-insensitive property of the CCPPS was further verified by numerical simulation as shown in Figure S6. The cross-section of the CCPPS was represented by a randomly distributed porous structure (micropore diameter = 300–500 μm, thickness of bridges = 50–100 μm), and the scale of the structure was modeled as the real size of the CCPPS-based pressure sensor. The bending-insensitive characteristics of the CCPPS originates from the nature of the microporous configuration. Since the change in overall arrangement of the microporous structure accommodates the bending-induced deformation of the entire sensor structure, the deformations of individual micropores are reduced with no significant distortion of the PDMS bridges surrounding the micropores. The local strain of most of the PDMS bridges inside the sensor structure was measured to be less than ~10% even at $r_{bending}$ < ~5 mm. Accordingly, contact between the micropores causing the current change does not noticeably occur under bent conditions. In addition, the reliability of CCPPS under dynamic bending stimulation were examined. In Figure 4b, the CCPPS-based pressure sensor was repeatedly bent to $r_{bending}$ of 28, 18, 16, and 14 mm, respectively. During the first 20 bending cycles, the base resistance was

almost completely returned to original values without a noticeable instability. The CCPPS-based pressure sensor showed an excellent long-term reliability with a negligible change of R_{base} and no structural failure after 1000 bending/release cycles, as shown in Figure 4c. Moreover, bending-insensitive pressure sensing capability of the CCPPS-based pressure sensor was investigated by comparing dynamic pressure responses under flat and bent conditions, as shown in Figure 4d. The responses under $r_{bending}$ of 50, 30 and 7.5mm were nearly identical to that of the flat condition, indicating that the pressure sensing performance of the sensor was not significantly affected by the bending-induced deformations. Such bending-insensitive pressure sensing capability enables the CCPPS-based pressure flexible sensor to accurately detect the normal forces or pressures even under bent situations in wearable human interface devices.

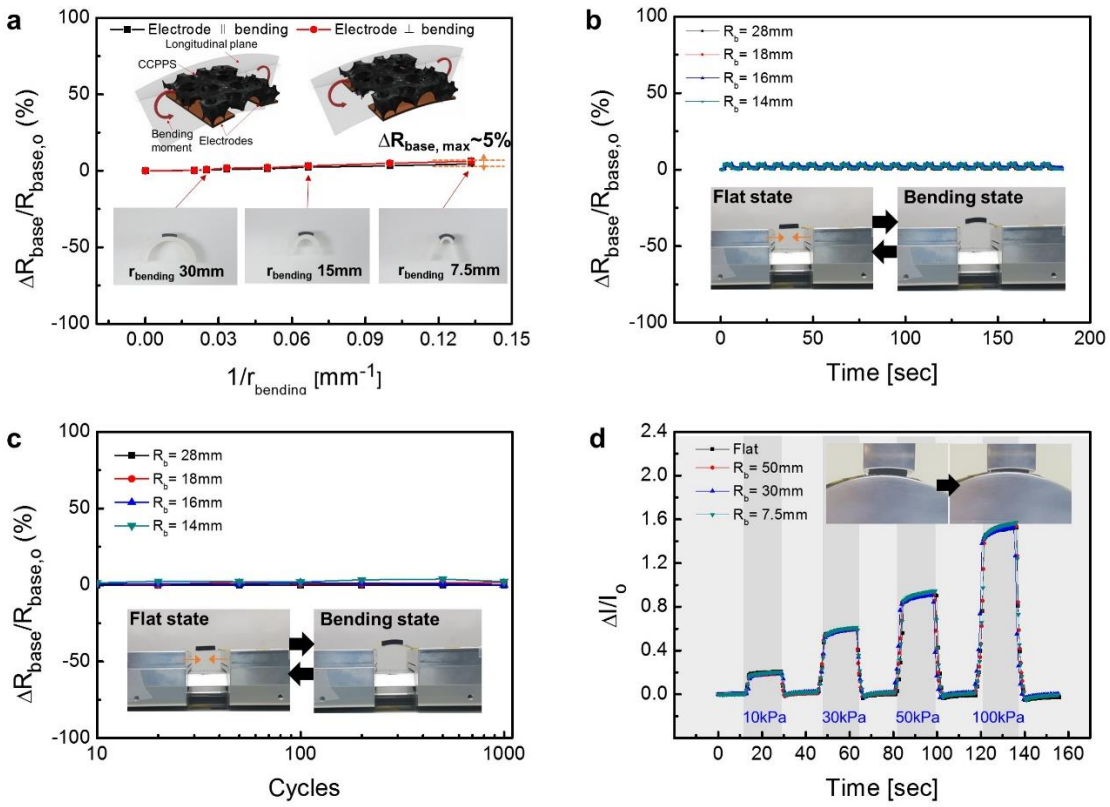

Figure 4 Bending-insensitivity of a CCPPS-based flexible pressure sensor under bent conditions: (a) Change of the base resistance of the pressure sensor with various bending radii from 50 to 7.5 mm for both cases of electrodes ∥ bending and electrodes ⊥ bending; (b) Recovery of the base resistance of the pressure sensor under repetitive dynamic bending cycles with the different bending radii (28, 18, 16, and 14 mm); (c) Long-term reliability of the pressure sensor during 1,000 bending cycles with the different bending radii (28, 18, 16, and 14 mm); (d) Comparison of the dynamic pressure responses of the pressure sensor under bent (50, 30, and 7.5 mm) and flat states, showing bending-insensitive pressure sensing capability.

A flexible piano pad based on the CCPPS-based flexible pressure sensor arrays was fabricated as a human interface device for an entertainment application. The flexible piano pad was designed to mimic a working principle of a real acoustic piano, where sound volumes can be controlled by the pressing speed of keyboards. Figure 5a shows a schematic illustration of a flexible piano pad, which is composed of 13 pressure sensor arrays-embedded keyboards. As shown in Figure 5b, the flexible piano pad exhibited excellent flexibility and robustness, since it was composed of soft elastomer (Ecoflex) and the CCPPS-based pressure sensors (Detailed fabrication procedures are described in Figure S7a and Experimental Section). Figure 5c shows a schematic illustration of voltage dividing circuits integrated within the keyboards for simultaneous measurement of 13 signals. Figure 5d shows a method for the conversion of voltage signals to the sound volumes in order to implement mimicking of the real acoustic piano. When the pressure sensors within the keyboards are pressed by human fingers, reference voltages (V_{ref}) increase with decreasing resistances of the pressure sensors (R_s). When the value of V_{ref} reaches the threshold voltage (V_{th}) at point A, the slope of the curve (dV_{ref}/dt) at this point is converted to the sound volume. In addition, the sound was programmed to be turned on only

when V_{ref} is higher than V_{th}. The sound volumes, which were simultaneously converted from 13 multiple channels, were output through the PC speaker as shown in Figure S7b. In order to evaluate the functionality, the sound volumes generated at different pressing speeds were compared. In Figure 5e, profiles of V_{ref} and the sound volume are represented by red and blue lines, respectively. It was clearly confirmed that as the pressing speed of the keyboards increases, increased slope of V_{ref} curve and sound volumes were produced (47, 85, and 118 *a.u.* for 10, 20, and 30 mm/sec, respectively) with a good linearity (Figure 5e and 5f). In addition, a variety of playing performance were evaluated by actually operating the flexible piano pad, as shown in Movie S3. In this video, the flexible piano pad obviously showed that the sound volume variation depends on the pressing speeds of the human fingers. Also, it was able to be played at a very fast tempo corresponding to "prestissimo (M.M. ♩=200)" due to the fast response of the CCPPS-based pressure sensor. The flexible piano pad facilitated a series of musical chord implementation, when several keyboards were pressed at the same time. Based on this basic playing performance, the famous music "Doremi Song" was successfully demonstrated.

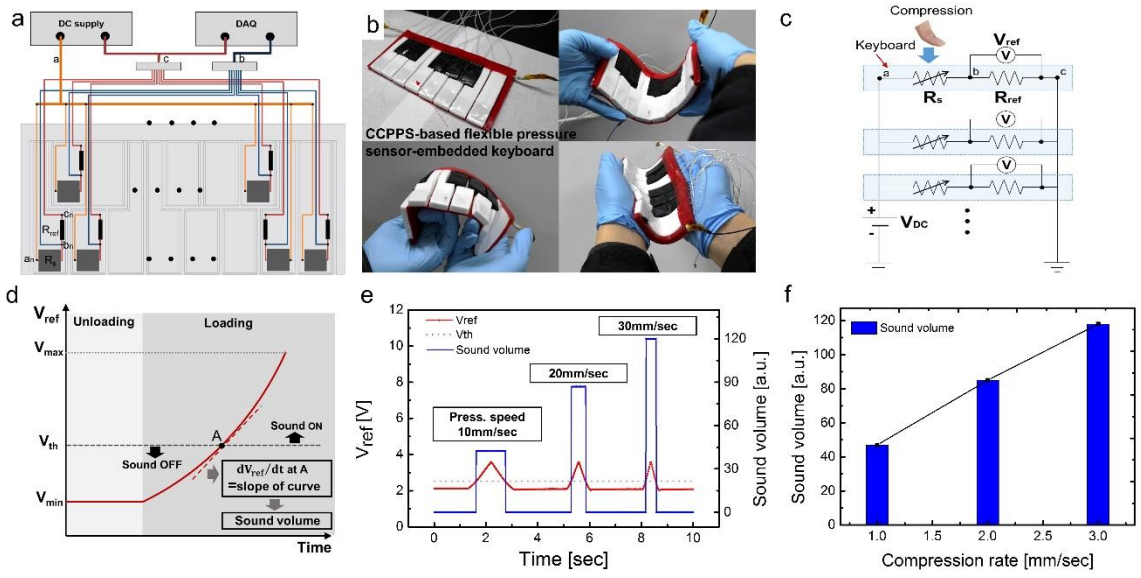

Figure 5 A flexible piano pad based on the CCPPS-based flexible pressure sensors, which mimics the principle of sound volume control of a real acoustic piano: (a) A schematic illustration of overall system of the flexible piano pad composed of the pressure sensor-embedded keyboards; (b) Photographic image of the fabricated flexible piano pad, showing its excellent flexibility and robustness; (c) Electrical circuits integrated in the keyboards for simultaneous measurement of the 13 multiple channels; (d) Method for the conversion of sensor signals to the sound volumes. The slope of voltage curve (dV_{ref}/dt) at point A is converted to the sound volume; (e, f) Sound volumes generated at different pressing speeds of the keyboard. As the pressing speed increased, the sound volume was also linearly increased (47, 85, and 118 *a.u.* for 10, 20, and 30 mm/sec, respectively).

As a wearable healthcare monitoring device, an in-shoe type flexible foot insole using the CCPPS-based flexible pressure sensor arrays was fabricated for real-time monitoring of foot plantar pressure distribution. Figure 6a displays a schematic illustration of the flexible foot insole. Ten CCPPS-based pressure sensor arrays were integrated on a flexible printed circuit board (FPBC) as shown Figure 6b. The pressure sensors were located on 10 critical positions, which support most of the body weights and adjust a body balance on foot anatomical areas[33]: fore-foot (#1–3), mid-foot (#4, 5, 9, and 10), and heel (#6–8). Individual sensors were packaged inside the sockets of a cover insole layer as depicted in Figure S8a. The two bottom electrode configuration led to a stable connection of the pressure sensors on the electrical circuits of the FPCB. Also, the pressure sensors allowed for accurate detection of local pressures without surrounding interference since the CCPPS does not suffer from barreling effect under compressive loading. The voltage outputs generated from 10 pressure sensors were transferred to a data acquisition (DAQ) board and were collected in a PC. In Figure 6c, the foot plantar

pressure measured by each sensor was displayed at corresponding positions of a 3D bar graph in a measurement program. Movie S4 shows a real-time change of the foot plantar pressure distribution according to the posture changes of a human body. The output of this device was in the form of a "pressure" in the measurement program, as shown in Figure 6c and Movie S4. This could offer more user-friendly and direct information, compared with most of the previous studies where the output was simply in the form of an "electrical signal". To implement this function, voltage signals were converted to the pressure values by the following steps (Figure S8b): (1) V_{ref} measured by the DAQ board were converted to $\Delta R/R_o$ using following equations, $\Delta R/R_o = (V_{in}/V_{ref} - 1) \times R_{ref}/R_o - 1$; (2) $\Delta R/R_o$ values were converted to the pressure values using calibration equations, $P = f(\Delta R/R_o) = a \times \exp(b \times \Delta R/R_o)$ (a and b are fitting constants), derived from fitting the experimental data, respectively. A gait motion of a 70 kg tester, wearing a shoe with the flexible foot insole, was evaluated by measuring the foot plantar pressure distribution. Figure 6d shows the pressure distribution over the entire foot plantar area under a standing stance. The 3D mapping clearly showed the pressure distribution related to the anatomical shape of foot plantar. High pressures were observed in the region of the fore-foot (# 1–3) and the heel (#8) primarily in contact with the insole, while relatively low pressures were measured in the mid-foot part with an arch shape (# 5, 10). Figures 6e and 6f display continuous curves of the pressure values measured at each position during walking and running for 5 steps, respectively. In Figure 6e, a peak value of # 8 was first observed, since the heel touched the ground at the beginning of the walking motions. In contrast, peak values of the fore-foot (# 1-3) were observed at the end of the walking motions. In Figure 6f, the peak values of all positions relatively increased with the time intervals between the peaks being decreased due to faster and more dynamic cyclic motions by running, compared with the walking. Accordingly, the flexible foot insole based on the CCPPS-based pressure sensors was capable of collecting the static and dynamic pressure data of human gait motion, which is applicable to

clinical or sports dynamics fields. The foot plantar pressure distribution data is one of the important indicators to diagnose and treat patients with diseases like obesity, diabetes or spinal diseases, *etc*.[33–35] Furthermore, this technique can be used for an assessment of athletic performance or rehabilitation by analyzing the gait patterns and speeds of athletes.

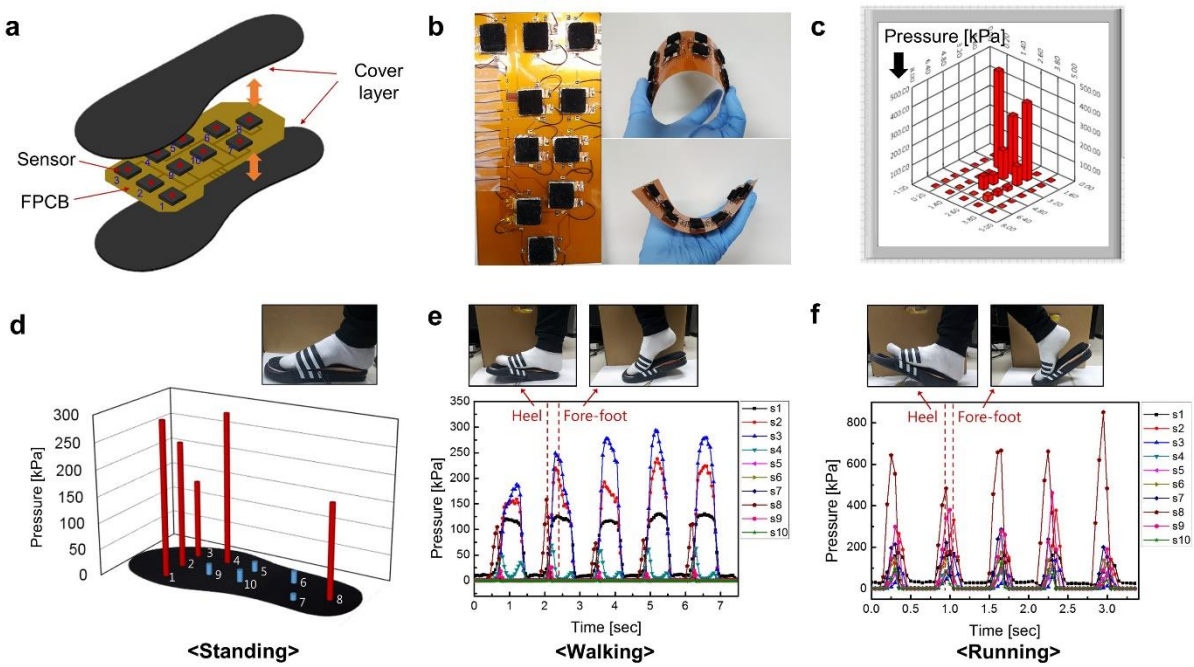

Figure 6 A flexible foot insole using the CCPPS based flexible pressure sensors for a real-time detection of foot plantar pressure distribution: (a) Schematic illustration of the flexible foot insole; (b) Photographic images of the fabricated pressure sensor-integrated FPCB; (c) 3D mapping of the foot pressure distribution in the measurement system; (d) Foot plantar pressure distribution during standing stance; (e, f) Dynamic changes of the pressures measured at each position during 5 steps of walking and running, respectively.

CONCLUSION

In summary, we developed a thin CCPPS-based flexible pressure sensor, which is capable of the ultrawide-pressure-range and bending-insensitive pressure sensing. Owing to the

gradual change of the contact between the CNT networks deposited on the micropores up to high compressive strain of the CCPPS, the pressure sensor operated in a very wide range from ultra-small to large pressures (10Pa–1.2MPa), with favorable sensitivity and high linearity maintained. Also, the CCPPS-based pressure sensor showed low hysteresis, fast dynamic responses, and long-term reliability due to the reversible and fully restored closure/opening of the micropores. The bending-insensitive pressure sensing capability of the CCPPS-based pressure sensor facilitates the accurate and stable detection of normal pressure under bent conditions. Accordingly, the thin CCPPS-based pressure sensor could be utilized for human interface device for entertainment and healthcare monitoring applications, respectively. In the future, our technology can be integrated with wireless system for a variety of applications, including portable human-machine interface devices, prosthetic skins, and mobile healthcare systems. Moreover, it is expected that the pressure sensing parameters could be precisely controlled and optimized by tuning the porosity, arrangement, and the size of the micropores of the CCPPS for a variety of wearable sensing applications.

ASSOCIATED CONTENT

Supporting Information. The following files are available free of charge via the internet at http://pubs.acs.org.

SEM and optical analysis of compressive behavior of a CNT-coated porous elastomer sponge (CCPPS), calculation of porosity of the CCPPS, simulation analysis of bending of the CCPPS; Table S1 and Figures S1-S8 (PDF)

Microcomputed tomography movie of the internal geometry of the CCPPS (AVI)

Gradual geometrical change of the microporous configuration of the CCPPS (AVI)

Demonstration of a playing performance of a flexible piano pad device (AVI)

Demonstration of a real-time 3D plotting of the foot pressure distribution (AVI)

AUTHOR INFORMATION

Corresponding Authors

*E-mail: Inkyu@kaist.ac.kr

*E-mail: Oyongsuk@kaist.ac.kr

Author Contributions

The manuscript was written through contributions of all authors. All authors have given approval to the final version of the manuscript.

Notes

ACKNOWLEDGMENT

This work was supported by the following research grants: (1) the National Research Foundation of Korea (NRF) grant funded by the Korea government(MSIT) (No. 2018R1A2B2004910); (2) the National Research Foundation of Korea(NRF) Grant funded by the Korean Government(MSIP) (No. 2015R1A5A1037668).

REFERENCES

(1) Someya, T.; Sekitani, T.; Iba, S.; Kato, Y.; Kawaguchi, H.; Sakurai, T. A Large-Area, Flexible Pressure Sensor Matrix with Organic Field-Effect Transistors for Artificial Skin Applications. *Proc. Natl. Acad. Sci.* **2004**, *101*, 9966–9970.

(2) Takei, K.; Takahashi, T.; Ho, J. C.; Ko, H.; Gillies, A. G.; Leu, P. W.; Fearing, R. S.; Javey, A. Nanowire Active-Matrix Circuitry for Low-Voltage Macroscale Artificial Skin. *Nat. Mater.* **2010**, *9*, 821–826.

(3) Hammock, M. L.; Chortos, A.; Tee, B. C. K.; Tok, J. B. H.; Bao, Z. 25th Anniversary Article: The Evolution of Electronic Skin (E-Skin): A Brief History, Design Considerations, and Recent Progress. *Adv. Mater.* **2013**, *25*, 5997–6038.

(4) Wang, X.; Dong, L.; Zhang, H.; Yu, R.; Pan, C.; Wang, Z. L. Recent Progress in Electronic Skin. *Adv. Sci.* **2015**, *2*, 1–21.

(5) Bauer, S.; Bauer-Gogonea, S.; Graz, I.; Kaltenbrunner, M.; Keplinger, C.; Schwödiauer, R. 25th Anniversary Article: A Soft Future: From Robots and Sensor Skin to Energy Harvesters. *Adv. Mater.* **2014**, *26*, 149–162.

(6) Trivedi, D.; Rahn, C. D.; Kier, W. M.; Walker, I. D. Soft Robotics: Biological Inspiration, State of the Art, and Future Research. *Appl. Bionics Biomech.* **2008**, *5*, 99–117.

(7) Lee, H.; Kwon, D.; Cho, H.; Park, I.; Kim, J. Soft Nanocomposite Based Multi-Point, Multi-Directional Strain Mapping Sensor Using Anisotropic Electrical Impedance Tomography. *Sci. Rep.* **2017**, *7*, 1–10.

(8) Schwartz, G.; Tee, B. C. K.; Mei, J.; Appleton, A. L.; Kim, D. H.; Wang, H.; Bao, Z. Flexible Polymer Transistors with High Pressure Sensitivity for Application in Electronic Skin and Health Monitoring. *Nat. Commun.* **2013**, *4*, 1858–1859.

(9) Boutry, C. M.; Nguyen, A.; Lawal, Q. O.; Chortos, A.; Rondeau-Gagné, S.; Bao, Z. A Sensitive and Biodegradable Pressure Sensor Array for Cardiovascular Monitoring. *Adv. Mater.* **2015**, *27*, 6954–6961.

(10) Zang, Y.; Zhang, F.; Di, C. A.; Zhu, D. Advances of Flexible Pressure Sensors toward Artificial Intelligence and Health Care Applications. *Mater. Horizons* **2015**, *2* , 140–156.

(11) Yang, Y.; Zhang, H.; Lin, Z. H.; Zhou, Y. S.; Jing, Q.; Su, Y.; Yang, J.; Chen, J.; Hu, C.; Wang, Z. L. Human Skin Based Triboelectric Nanogenerators for Harvesting Biomechanical Energy and as Self-Powered Active Tactile Sensor System. *ACS Nano* **2013**, *7*, 9213–9222.

(12) Zhu, G.; Yang, W. Q.; Zhang, T.; Jing, Q.; Chen, J.; Zhou, Y. S.; Bai, P.; Wang, Z. L. Self-Powered, Ultrasensitive, Flexible Tactile Sensors Based on Contact Electrification. *Nano Lett.* **2014**, *14*, 3208–3213.

(13) Wang, S.; Lin, L.; Wang, Z. L. Triboelectric Nanogenerators as Self-Powered Active Sensors. *Nano Energy* **2015**, *11*, 436–462.

(14) Takamatsu, S.; Yamashita, T.; Imai, T.; Itoh, T. Lightweight Flexible Keyboard with a Conductive Polymer-Based Touch Sensor Fabric. *Sensors Actuators, A Phys.* **2014**, *220*, 153–158.

(15) Lipomi, D. J.; Vosgueritchian, M.; Tee, B. C. K.; Hellstrom, S. L.; Lee, J. A.; Fox, C. H.; Bao, Z. Skin-like Pressure and Strain Sensors Based on Transparent Elastic Films of Carbon Nanotubes. *Nat. Nanotechnol.* **2011**, *6*, 788–792.

(16) Mannsfeld, S. C. B.; Tee, B. C.-K.; Stoltenberg, R. M.; Chen, C. V. H.-H.; Barman, S.; Muir, B. V. O.; Sokolov, A. N.; Reese, C.; Bao, Z. Highly Sensitive Flexible Pressure Sensors with Microstructured Rubber Dielectric Layers. *Nat. Mater.* **2010**, *9*, 859.

(17) Xiao, X.; Yuan, L.; Zhong, J.; Ding, T.; Liu, Y.; Cai, Z.; Rong, Y.; Han, H.; Zhou, J.; Wang, Z. L. High-Strain Sensors Based on ZnO Nanowire/Polystyrene Hybridized Flexible Films. *Adv. Mater.* **2011**, *23*, 5440–5444.

(18) Lozano-Pérez, C.; Cauich-Rodríguez, J. V.; Avilés, F. Influence of Rigid Segment and Carbon Nanotube Concentration on the Cyclic Piezoresistive and Hysteretic Behavior of Multiwall Carbon Nanotube/Segmented Polyurethane Composites. *Compos. Sci. Technol.* **2016**, *128*, 25–32.

(19) Zhang, R.; Deng, H.; Valenca, R.; Jin, J.; Fu, Q.; Bilotti, E.; Peijs, T. Strain Sensing Behaviour of Elastomeric Composite Films Containing Carbon Nanotubes under Cyclic Loading. *Compos. Sci. Technol.* **2013**, *74*, 1–5.

(20) Choong, C. L.; Shim, M. B.; Lee, B. S.; Jeon, S.; Ko, D. S.; Kang, T. H.; Bae, J.; Lee, S. H.; Byun, K. E.; Im, J.; et al. Highly Stretchable Resistive Pressure Sensors Using a Conductive Elastomeric Composite on a Micropyramid Array. *Adv. Mater.* **2014**, *26*, 3451–3458.

(21) Qi, K.; He, J.; Wang, H.; Zhou, Y.; You, X.; Nan, N.; Shao, W.; Wang, L.; Ding, B.; Cui, S. A Highly Stretchable Nanofiber-Based Electronic Skin with Pressure-, Strain-, and Flexion-Sensitive Properties for Health and Motion Monitoring. *ACS Appl. Mater. Interfaces* **2017**, *9*, 42951–42960.

(22) Pang, C.; Lee, G. Y.; Kim, T. Il; Kim, S. M.; Kim, H. N.; Ahn, S. H.; Suh, K. Y. A Flexible and Highly Sensitive Strain-Gauge Sensor Using Reversible Interlocking of Nanofibres. *Nat. Mater.* **2012**, *11*, 795–801.

(23) Gong, S.; Schwalb, W.; Wang, Y.; Chen, Y.; Tang, Y.; Si, J.; Shirinzadeh, B.; Cheng, W. A Wearable and Highly Sensitive Pressure Sensor with Ultrathin Gold Nanowires. *Nat. Commun.* **2014**, *5*, 1–8.

(24) Yao, H. Bin; Ge, J.; Wang, C. F.; Wang, X.; Hu, W.; Zheng, Z. J.; Ni, Y.; Yu, S. H. A Flexible and Highly Pressure-Sensitive Graphene-Polyurethane Sponge Based on Fractured Microstructure Design. *Adv. Mater.* **2013**, *25*, 6692–6698.

(25) Pang, Y.; Tian, H.; Tao, L.; Li, Y.; Wang, X.; Deng, N.; Yang, Y.; Ren, T. L. Flexible, Highly Sensitive, and Wearable Pressure and Strain Sensors with Graphene Porous Network Structure. *ACS Appl. Mater. Interfaces* **2016**, *8*, 26458–26462.

(26) Zhang, H.; Liu, N.; Shi, Y.; Liu, W.; Yue, Y.; Wang, S.; Ma, Y.; Wen, L.; Li, L.; Long, F.; et al. Piezoresistive Sensor with High Elasticity Based on 3D Hybrid Network of Sponge@CNTs@Ag NPs. *ACS Appl. Mater. Interfaces* **2016**, *8*, 22374–22381.

(27) Han, J. W.; Kim, B.; Li, J.; Meyyappan, M. Flexible, Compressible, Hydrophobic, Floatable, and Conductive Carbon Nanotube-Polymer Sponge. *Appl. Phys. Lett.* **2013**, *102*, 051903.

(28) Iglio, R.; Mariani, S.; Robbiano, V.; Strambini, L.; Barillaro, G. Flexible Polydimethylsiloxane Foams Decorated with Multiwalled Carbon Nanotubes Enable Unprecedented Detection of Ultralow Strain and Pressure Coupled with a Large Working Range. *ACS Appl. Mater. Interfaces* **2018**, *10*, 13877–13885.

(29) Lee, S.; Reuveny, A.; Reeder, J.; Lee, S.; Jin, H.; Liu, Q.; Yokota, T.; Sekitani, T.; Isoyama, T.; Abe, Y.; et al. A Transparent Bending-Insensitive Pressure Sensor. *Nat. Nanotechnol.* **2016**, *11*, 472–478.

(30) Chen, S.; Zhuo, B.; Guo, X. Large Area One-Step Facile Processing of Microstructured Elastomeric Dielectric Film for High Sensitivity and Durable Sensing over Wide Pressure Range. *ACS Appl. Mater. Interfaces* **2016**, *8*, 20364–20370.

(31) Graz, I.; Krause, M.; Bauer-Gogonea, S.; Bauer, S.; Lacour, S. P.; Ploss, B.; Zirkl, M.; Stadlober, B.; Wagner, S. Flexible Active-Matrix Cells with Selectively Poled Bifunctional Polymer-Ceramic Nanocomposite for Pressure and Temperature Sensing Skin. *J. Appl. Phys.* **2009**, *106*, 034503.

(32) Kwon, D.; Lee, T. I.; Shim, J.; Ryu, S.; Kim, M. S.; Kim, S.; Kim, T. S.; Park, I. Highly Sensitive, Flexible, and Wearable Pressure Sensor Based on a Giant Piezocapacitive Effect of Three-Dimensional Microporous Elastomeric Dielectric Layer. *ACS Appl. Mater. Interfaces* **2016**, *8*, 16922–16931.

(33) Abdul Razak, A. H.; Zayegh, A.; Begg, R. K.; Wahab, Y. Foot Plantar Pressure Measurement System: A Review. *Sensors (Switzerland)* **2012**, *12*, 9884–9912.

(34) Hills, Andrew P, H. E. M. Plantar Pressure Differences between Obese and Non-Obese Adults: A Biomecha...: Discover GALILEO. *Int. J. Obes. Relat. Metab. Disord.* **2001**, 1674.

(35) Paton, J.; Bruce, G.; Jones, R.; Stenhouse, E. Effectiveness of Insoles Used for the Prevention of Ulceration in the Neuropathic Diabetic Foot: A Systematic Review. *J. Diabetes Complications* **2011**, *25*, 52–62.

Table of Contents Graphic